The benefits of turbine endwall profiling in a cascade

G Ingram[1], **D Gregory-Smith**[1]*, and **N Harvey**[2]
[1]University of Durham, School of Engineering, Durham, UK
[2]Rolls-Royce plc, Derby, UK

The manuscript was received on 14 May 2004 and was accepted after revision for publication on 5 August 2004.

DOI: 10.1243/095765005X6863

Abstract: Non-axisymmetric profiled endwalls have been shown to reduce losses and secondary flow both in cascades and in rig tests. This paper presents experimental results which quantify the benefits of loss reduction in the cascade with particular attention to accuracy. The paper compares the benefits achieved in experiment to the results predicted by computational fluid dynamics (CFD). The results show that both the experiment and CFD give significant reductions in secondary flow. A reduction of 31 per cent in secondary loss has been measured for the best case, but the CFD gives only a small reduction in loss. Previous studies on the planar endwall have shown significant areas of transitional flow, so the surface flow has been studied with the aid of surface-mounted hot films. It was concluded that the loss reductions were not due to changes in regions of laminar and turbulent flow.

Keywords: turbine blades, secondary flow, endwall profiling, experiment, CFD

1 INTRODUCTION

Three-dimensional non-axisymmetric endwall profiling has been shown to reduce secondary loss using a number of different geometries. Sieverding [**1**] provided an excellent review of secondary flows, the fundamentals of which are not discussed in this paper. Harvey *et al.* [**2**] and Hartland *et al.* [**3**] described the design and testing of a profiled end wall geometry for a low-speed linear cascade (the so-called Durham cascade); they showed a reduction in overall loss of some 20 per cent of the planar value. Yan *et al.* [**4**] showed a reduction of 4 per cent in overall loss for a steam turbine nozzle geometry in a linear cascade. Brennan *et al.* [**5**] and Rose *et al.* [**6**] designed and tested three-dimensional non-axisymmetric endwalls for the HP turbine of the Rolls-Royce Trent 500 in an engine representative rig. They reported a stage efficiency improvement of 0.59 per cent. More recently, Harvey *et al.* [**7**] validated endwall profiling in a multiple blade row environment and Ingram *et al.* [**8**] examined the reasons behind the improvement in performance.

Put simply, non-axisymmetric endwall profiling works by reducing the cross passage pressure gradient at the endwall by means of streamline curvature. This reduced pressure gradient then results in less secondary flow and therefore loss. In reality the picture is complicated by the fact there are multiple vortical structures in even cascade secondary flow [**1**] and the flow is transitional [**9**] but the reduced cross passage pressure gradient is the design aim. See Ingram *et al.* [**8**] for more details on how endwall profiling affects the flow structure.

This paper attempts to quantify the benefits of non-axisymmetric endwalls when applied to a turbine cascade and examine how well the computational fluid dynamics (CFD) solution used in the design of the profiles has predicted the actual flow. Providing an accurate and repeatable quantitative measurement of endwall performance is difficult and this paper describes methodologies developed at Durham to do just that.

Previous studies on the planar endwall [**9**] have shown significant areas of transitional flow, so the surface flow has been studied with the aid of surface mounted hot films. If the loss reductions associated with endwall profiling are due to changing the nature of the blade surface boundary layer, the performance gains may not be transferable to all machines. If on the other hand the loss reductions associated with endwall profiling are due to reduced

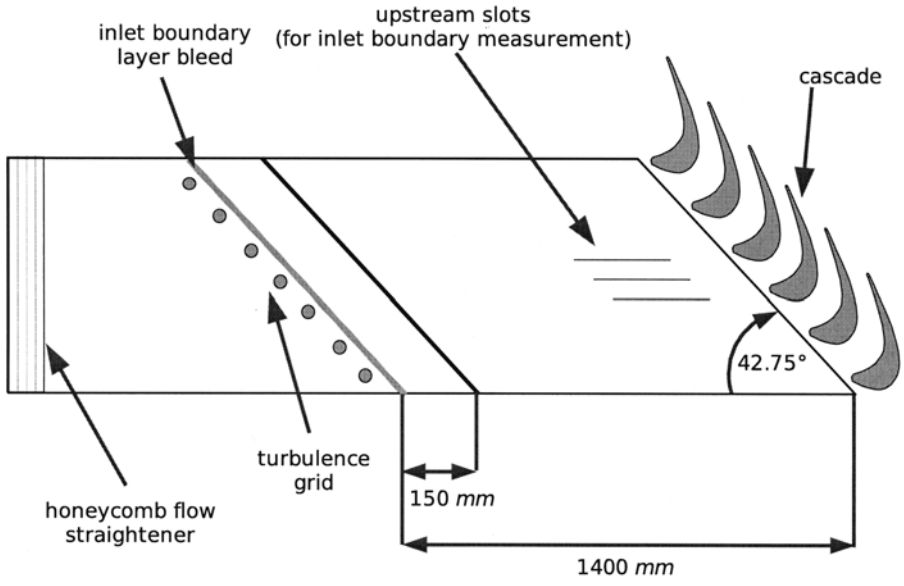

Fig. 1 Cascade layout

passage vortex strength then the benefits of endwall profiling will be more generally applicable.

2 EXPERIMENTAL TECHNIQUE

The Durham cascade is a low-speed, large-scale linear cascade of six rotor blades taken from a high-pressure rotor design. The cascade is shown in Fig. 1. A grid of bars mounted 1400 mm in front of the blades gives a turbulence intensity of around 5 per cent at the inlet. A boundary layer bleed is provided before the cascade is reached. The design data for the cascade are given in Table 1. The aerofoil has an aspect ratio of 1.78, which means there is a large region of undisturbed mid-span flow. Therefore the secondary flow regions on each endwall of the cascade do not interfere with each other. The blades are cantilevered from one endwall, into which slots are cut to provide access for measurement probes. Only one passage is instrumented. The other endwall consists of a series of panels, each of which cover a blade passage. These panels can be either profiled or flat. Measurements are taken in half the blade passage.

The rig is set to operate as close as possible to the correct Reynolds number; the speed of the airflow through the tunnel is adjusted to compensate for variations in atmospheric conditions. All the pressure probe readings are compensated to standard day conditions, so that readings from different days can be compared with one another.

Two generations of endwall design are described in this paper, *P*1 (first-generation), with profiling extending throughout the computational domain, and *P*2, with profiling restricted to just the blade passage. The planar endwall is termed *P*0. Endwall geometries are shown in Fig. 2. The contours represent height deviations from the planar case and are in mm. As well as the 'hump and dip' combination necessary to reduce the cross passage pressure gradient, the *P*1 geometry features an additional ridge on the suction side of the passage near the trailing edge. This was designed to reduce the overturning at the wall by introducing an enhanced counter corner vortex. Figure 3 shows some three dimensional views of the endwalls to aid visualization of the profile shapes.

The bulk of the results in this paper were taken using conventional five- and three-hole probes to obtain velocity components and loss. In this paper measurements are only presented at the axial plane used for reference, which is 28 per cent of an axial chord downstream of the trailing edge.

Endwall profiling also has the general effect of keeping the secondary loss and flow much closer to the endwall [**10**]. This means that it is important to measure the boundary layer as well as the bulk flow at the measurement plane. For five-hole probe measurements the closest point to the endwall was

Table 1 Design data for the Durham cascade

Inlet flow angle	42.75°
Blade exit angle	−68.7°
Blade chord	224 mm
Blade axial chord	181 mm
Blade pitch	191 mm
Blade half-span	200 mm
Reynolds number (axial chord and exit velocity)	4.0×10^5

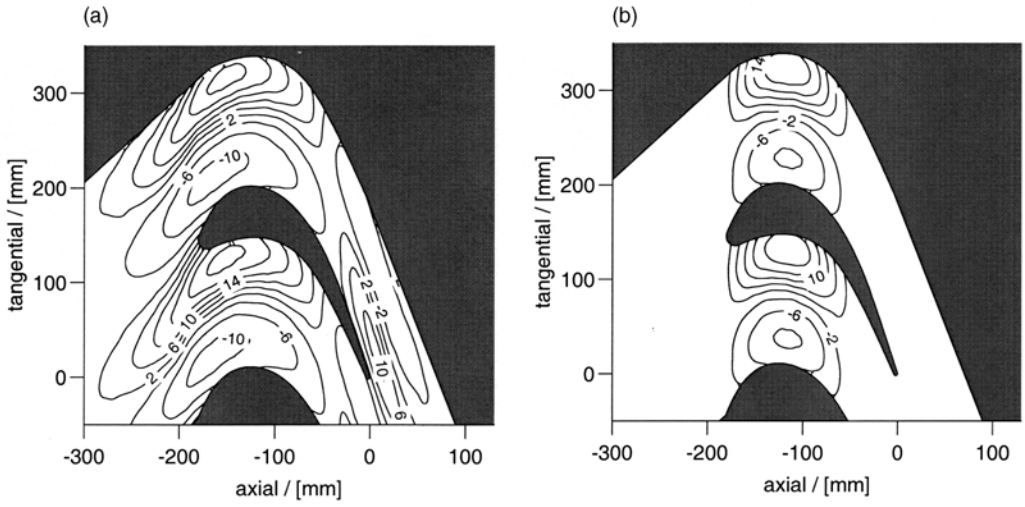

Fig. 2 Endwall geometries: (a) *P*1 geometry; (b) *P*2 geometry

5 mm so a three-hole probe was used to capture important information close to the wall.

Measurement grids have to be adjusted to accommodate the curvature of the endwall at the measurement plane. There is a uniform tangential spacing of 7 mm. For five-hole traverses, radial steps of 5 mm were used from 5 to 100 mm, and above 100 mm a 10 mm spacing was used. The contoured grids are generated so that the perturbations from the endwall reduce towards mid-span. For the three-hole probe, radial steps of 1 mm were used from 1 to 5 mm.

3 EXPERIMENTAL METHODOLOGY

The technique used for five-hole and three-hole probe measurements was essentially the same as that described in Treaster and Yocum [**11**]. Data acquisition was automated and a mechanised traverse gear moved the probe without human intervention. This high level of automation allowed a relatively large number of traverses to be conducted.

Before commencing readings, the operation of all the logging programs, transducers, probe, and the most significant data processing programs was tested. Essentially a series of readings were carried out at a number of known angles and at zero loss. The closeness to which the measurement system returns the angles and zero loss gives an indication of the errors in the system. The test was also repeated after a given set of readings, to ensure no degradation in the system had taken place during the tests.

The logging software contained two notable subroutines, which improved the quality of the experimental results. The first checked to ensure that the reading had settled after the probe had been moved through a flow field. Secondly, the data from each

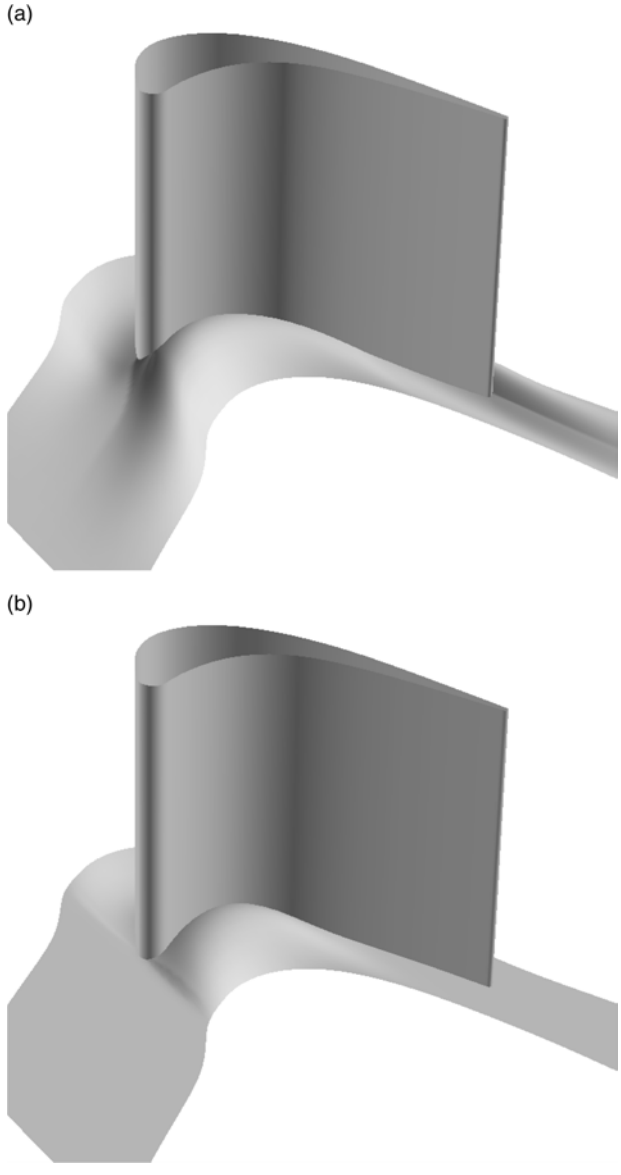

Fig. 3 (a) *p*1 geometry in 3D; (b) *p*2 geometry in 3D

measurement point underwent a statistical test to eliminate measurements with too much scatter in the data.

The other key element in achieving good quantitative results is to achieve consistency in the process used to collect the results. To achieve this, the tests for each endwall were conducted sequentially. In fact the probe starting position was set and locked in place; each endwall was inserted and tested in turn in a 'back to back' manner. This means that variations in probe positioning etc. did not affect the results.

The planar geometry was already quite efficient and the ranking of competing geometries required even more precision in the total pressure measurement. The difference in total pressure loss between the profiled endwalls is of the order of a few Pascals. The loss changes are very small in absolute terms. In order to provide 'definitive' results, the cascade traverses have been conducted three times; the differences between each of these traverses give some idea of the repeatability of the experiment and the average provides the 'definitive' result.

3.1 Transitional flow studies

Surface-mounted hot films were used to examine the effect endwall profiling has on the transitional nature of the flow. Measurements have been conducted both on the blade surfaces and on the endwalls. A detailed explanation of the experimental technique may be found in Ingram [**12**].

4 RESULTS

Contour plots of loss coefficient are presented for five- and three-hole probe readings. These area plots show the results of averaging three separate traverses for each endwall geometry ($P0$, $P1$, and $P2$). Repeating the experiment also allows an estimate of the accuracy of the final result to be made. The difference between the averaged area plots and individual area plots is very small and so is not shown. For all the traverses at 128% C_{ax} there is an overlap in the tangential direction of approximately 0.3 blade pitch.

4.1 Five-hole probe results for 128 per cent C_{ax}

Figure 4 shows the secondary vectors for the three cases. Secondary vectors are defined as deviations from the 2D midspan flow. The planar case (Fig. 4a) exhibits a classic secondary flow pattern with a large passage vortex located around $t = -250$ mm, $r = 60$ mm. A smaller vortex associated with the suction side of the horseshoe vortex and the trailing filament vorticity is located above and to the left of the main passage vortex at $t = -290$ mm, $r = 90$ mm. The counter corner vortex is also just visible at $t = -310$ mm, $r = 10$ mm.

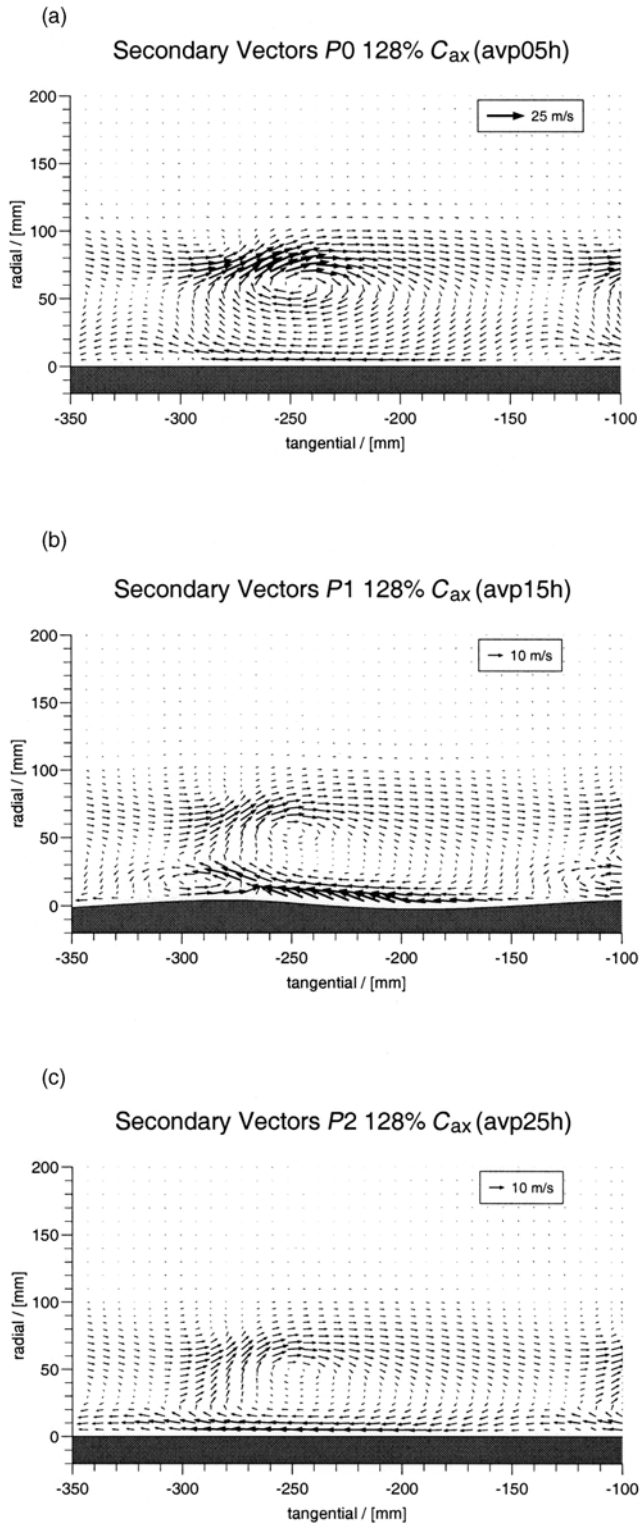

Fig. 4 Secondary velocity vectors at 128 per cent C_{ax}

Figure 4b and c shows the changes that endwall profiling introduces to the secondary flow field. For $P1$ the passage vortex is smaller and closer to the endwall and the enhanced counter corner vortex can also be clearly seen at $t = -290$ mm, $r = 15$ mm. For $P2$ the passage vortex is again smaller and closer to the endwall; however, the overturning near the endwall appears slightly greater for the profiled case than for the planar case.

Figure 5a–c shows the loss coefficients for $P0$, $P1$, and $P2$, respectively. $P1$ and $P2$ reduce secondary flow and loss, with the passage vortex loss cores in Fig. 5b and c being smaller than those in Fig. 5a. In general, profiled endwalls increase the overturning at the endwalls. However, $P1$ does not increase overturning with respect to the planar case. This is at the expense of greater loss locally, as the enhanced corner vortex generates a large amount of loss.

4.2 Three-hole probe results for 128 per cent C_{ax}

Figure 6a shows close wall loss coefficient contours for $P0$ at 128 per cent C_{ax}. Figure 6b and c shows the close wall loss coefficient for $P1$ and $P2$, respectively. Note the expanded radial scale and the fact that the profiling for $P1$ extends to beyond 128 per cent C_{ax}. Once again, the values shown are averaged values of three separate traverses. The area plots show clearly the large region of increased loss associated with the enhanced corner vortex for $P1$, although the increased overturning for P2 does not manifest itself as increased loss compared with the planar case.

4.3 Pitch averaged results for 128 per cent C_{ax}

Figure 7 shows the secondary kinetic energy coefficient at 128 per cent C_{ax}. This figure shows the significant reductions in C_{ske} that are obtained with profiled endwalls. In essence, Fig. 7 is a pitch-averaged representation of the secondary flow dynamics seen in Fig. 4. As can be seen from the figure the second generation endwall has the greatest C_{ske} reduction. Area-averaged values of C_{ske} are included in Table 2, showing that the profiling reduces the C_{ske} by about 50 per cent.

As discussed above each profile has three measurements taken at 128 per cent C_{ax}. Each of these measurements was conducted from scratch each time, that is they were taken on different days and all the equipment was reset between traverses. So for each set of readings the tangential position and yaw angle of the probe were reset. This allows us to quantify the repeatability of the experiments and estimate the effects of probe setting variation, etc. The variation on area plots is very small between traverses; however a small amount of variation can

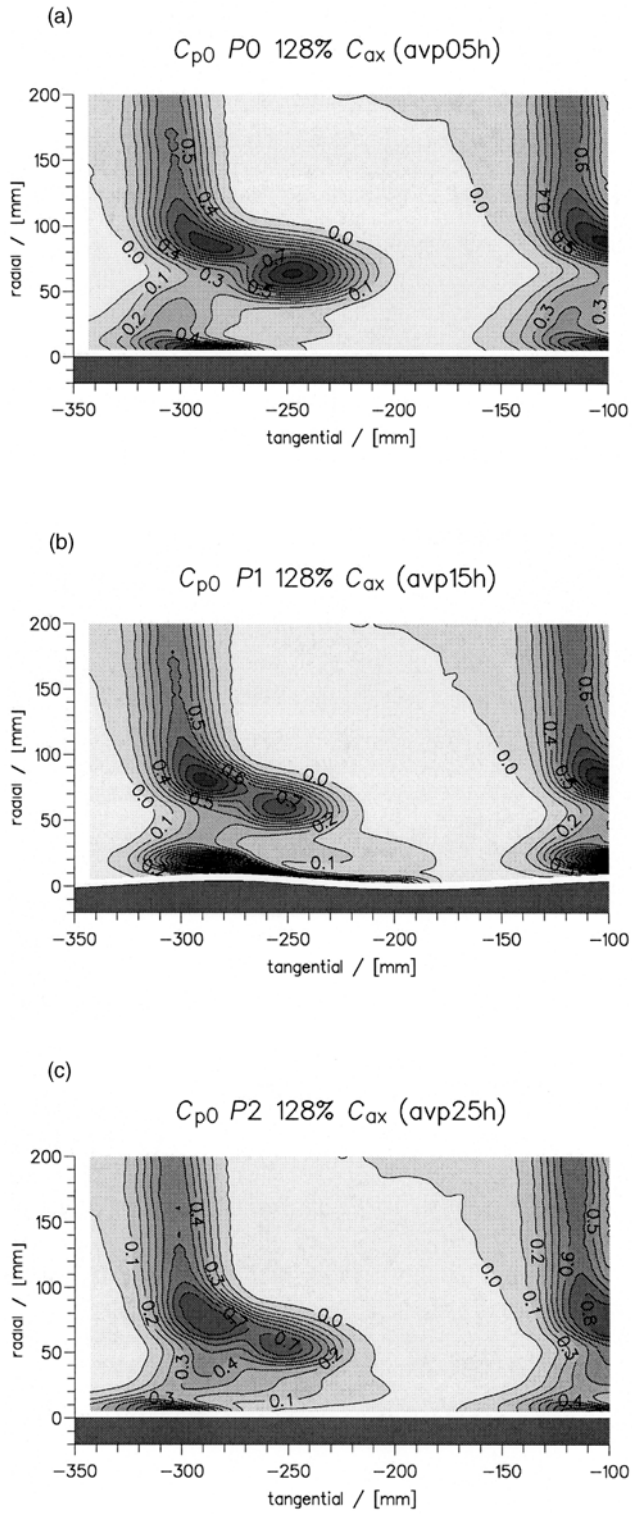

Fig. 5 Loss coefficient at 128 per cent C_{ax}

be seen in the pitch averaged plots. An example of the pitch-averaged loss variation is shown in Fig. 8, obtained with the five-hole probe. The degree of variation appears to be very small with extremely good qualitative agreement between the traverses. A full examination of the results shows that the

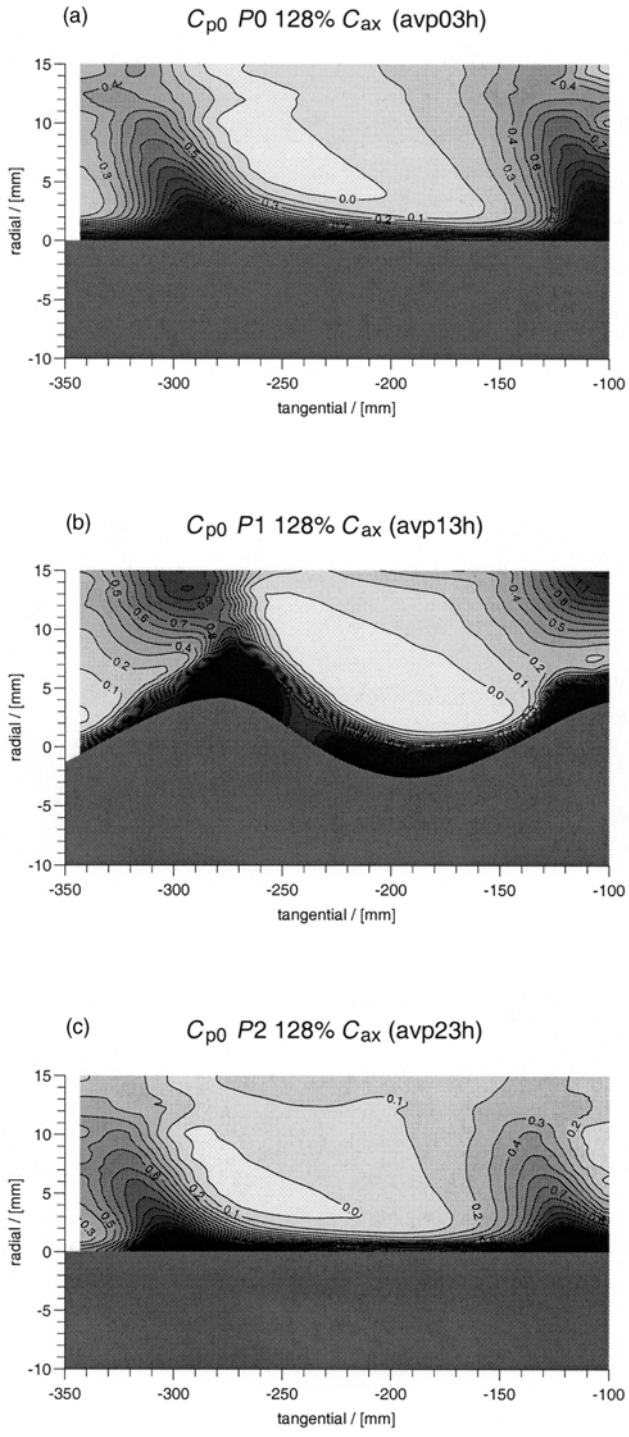

Fig. 6 Close wall loss coefficient at 128 per cent C_{ax}

maximum loss difference is over 0.1, but this is for only one point close to the endwall on *P*1 (not shown) and a much more typical value would be 0.02. Although not shown here, yaw angle agreement is excellent with all angles within half a degree of each other [**12**].

Area averaged results are shown in Table 2 as well as in Fig. 9. The level of variation in loss results is

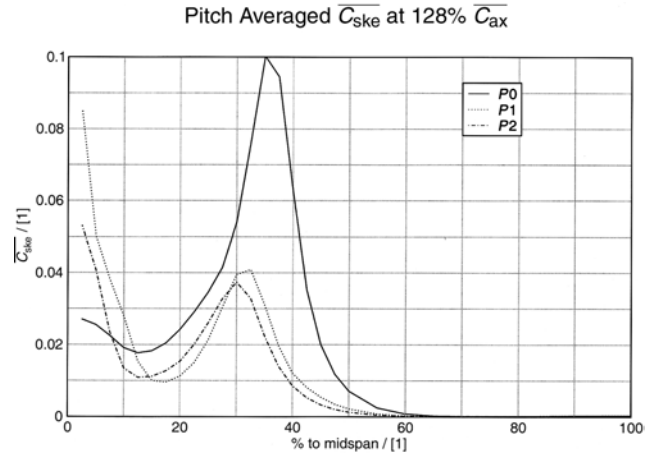

Fig. 7 Pitch-averaged C_{ske} at 128 per cent C_{ax}

quite surprising given the good agreement that is apparently present in the pitch-averaged results. For example, the planar secondary loss maximum variation between different traverses is some 3.6 per cent of the mean value, which seems quite high when compared to the pitch averaged plots. For each set of readings for *P*0, *P*1, and *P*2, the mean and standard deviation was taken and twice the largest standard deviation for the total and secondary loss calculation is used for the error bars. The error bars used in Fig. 9 are therefore set to 0.005. Should repeated loss measurements follow a normal distribution, this means that the mean value plus or minus two standard deviations should encompass 95.5 per cent of all readings. Obviously with such a small sample size such statistical methods are somewhat suspect as a single 'rogue' value will have a big effect, but this is at least a rational way of assessing the error associated with endwall measurements that can be logically extended should further experiments be conducted. Table 2 lists the mean and error margins for loss measurements associated with the three endwalls. The mean net secondary loss is also plotted in Fig. 9. Significantly it is apparent both profile losses will offer improvements over the planar case, but that the error bars for the *P*1 and *P*2 cases overlap.

Table 2 Mean loss and error estimate for five-hole probe readings

	*P*0	*P*1	*P*2	Error
Total loss	0.1503	0.1336	0.1289	±0.005
Secondary loss	0.0723	0.0554	0.0517	±0.004
Percentage planar loss	100.0	76.5	71.4	±5.1
C_{ske}	0.0203	0.0110	0.0092	–
C_{ske} percentage planar	100.0	54.0	45.5	–

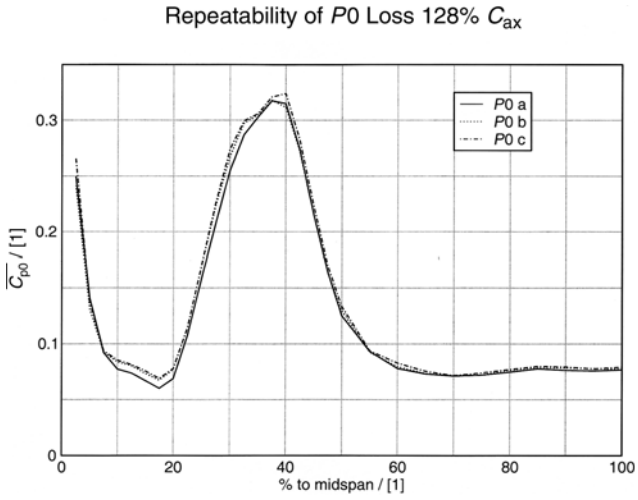

Fig. 8 Repeatability of pitch-averaged loss

A similar exercise in repeating the measurements at 128 per cent C_{ax} was conducted for three-hole probe results as for the five-hole probe results. In general similar results were obtained, with the pitch averaged values showing good agreement but the area-averaged values showing several percentage points of variation between different measurements. Three-hole probe area-averaged numbers are shown in Table 3, which covers a radial extent of 0–15 mm.

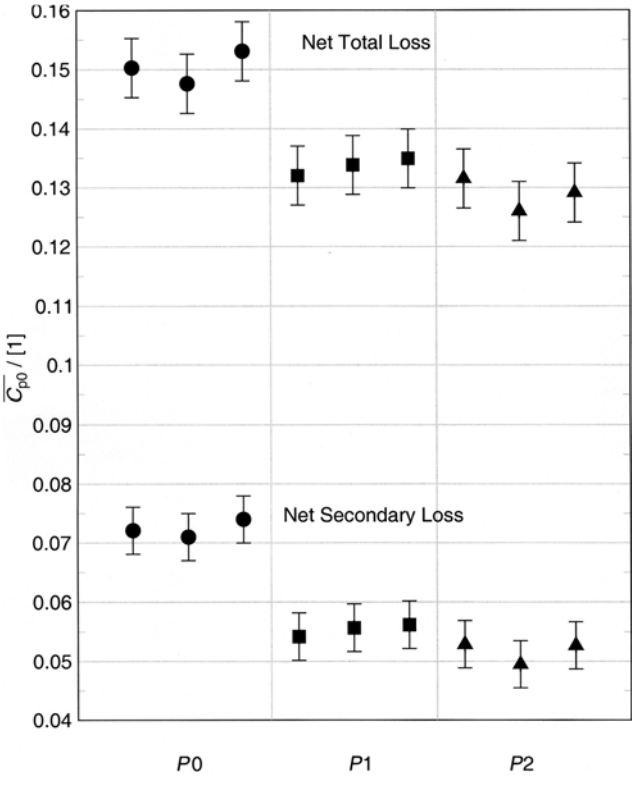

Fig. 9 Area-averaged loss coefficients (five-hole probe)

Table 3 Mean loss and error estimate for three-hole probe readings

	*P*0	*P*1	*P*2	Error
Gross loss, $\overline{\overline{C_{p0}}}$	0.3069	0.4149	0.2441	±0.04
Percentage planar loss	100.0	135.2	79.5	±13.0

The three-hole probe area-averaged loss results are the gross figures, i.e. without the inlet boundary layer subtracted, as subtracting either the whole boundary layer or only the first 15 mm from the three-hole probe does not have much physical meaning. The error estimate is calculated in an identical manner as for the five-hole probe.

The *P*1 profile has the largest loss, which is expected given the existence of the enhanced corner vortex. The *P*2 geometry actually results in a reduction in loss at the endwall. Clearly the enhanced corner vortex is a major loss-producing feature, but the increased cross flow in *P*2 does not appear to be contributing to increased loss compared to the planar case. This is significant as Harvey *et al.* [**2**] point out one of the effects of endwall profiling in general is to increase the overturning at the endwall.

4.4 Synthesized data set

In order to obtain the best measurement of the change in loss between endwalls of different design, the three- and five-hole averaged data sets are combined to produce a synthesized data set. This data set consists of the three-hole readings up to and including 5 per cent of span, $r = 10$ mm for a planar wall – the remainder of the data set is taken up by five-hole probe readings. Figure 10 shows the

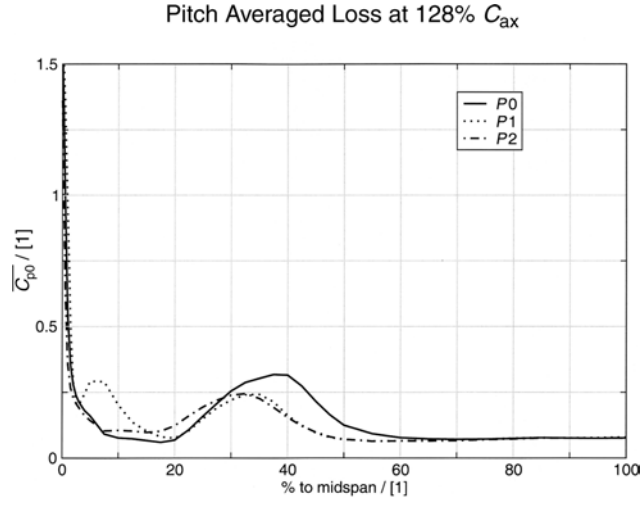

Fig. 10 Three- and five-hole results combined

pitch-averaged loss. The near wall loss is very high compared with the passage vortex loss core but the percentage span that it covers is quite small.

The synthesized data set is mainly intended to examine the changes in the area averaged values caused by including the three-hole probe measurements. When the three-hole probe measurements are included, the *P*1 data increase by a greater amount than the *P*2 data set. This is shown in Table 4, which contains values for the synthesized data set. Figure 11 shows the net secondary loss of the combined data set along with error bars taken from the five-hole data set. Figure 11 also shows the change in secondary loss for each of the geometries when the three-hole readings are included.

Including the close wall readings captures more of the loss of the *P*1-enhanced corner vortex and the fact that *P*2 has a lower close wall loss than the planar case means that the apparent performance of *P*2 relative to the datum is improved. If the error estimates are kept the same as for the five-hole probe, the difference in secondary loss values for *P*1 and *P*2 are now greater than the expected range of experimental error.

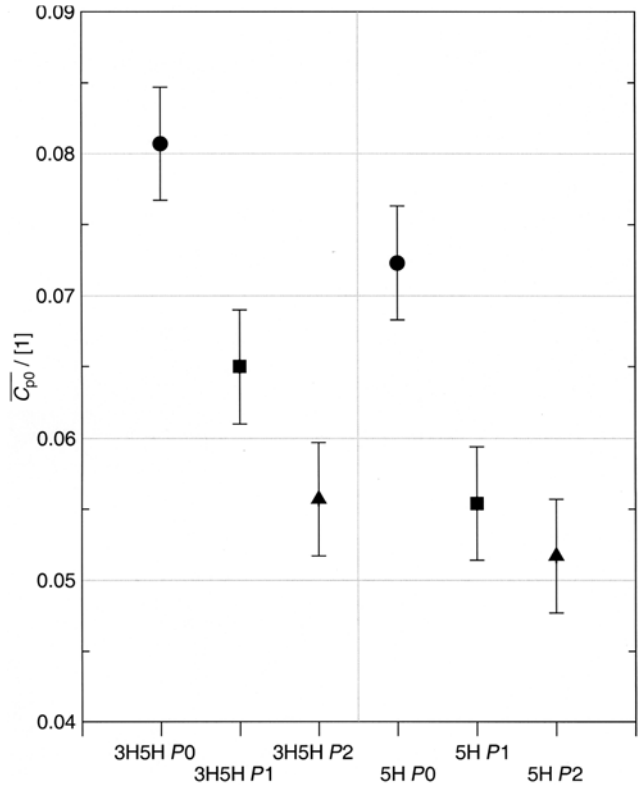

Fig. 11 Area-averaged secondary loss of the combined and five-hole-only data

5 COMPUTATIONAL FLUID DYNAMICS

The design work on the profiles was carried out using one of the turbomachinery CFD codes of Rolls-Royce, based on the pressure correction algorithm of Moore [**13**]. The grid consisted of a modest number of points (approximately 100 000) as during the design the calculation has to be repeated many times. An algebraic mixing length model and wall functions are used to model the flow. All surfaces are modelled as fully turbulent, as this would be the practice used in a real design calculation. Further details may be found in Harvey *et al.* [**2**].

The same processing was applied to CFD data as experimental data for this paper. Data points were extracted from the CFD solution at the measurement grid locations. These CFD points were then placed in a file in experimental format, then processed as if they were experimental results. This ensured that the results were directly comparable.

Table 4 Combined three- and five-hole probe loss readings

	*P*0	*P*1	*P*2	Error
Total loss, $\overline{\overline{C_{p0}}}$	0.1574	0.1431	0.1322	±0.005
Secondary loss	0.0807	0.0650	0.0557	±0.004
Percentage planar loss	100.0	80.5	69.0	±5.1

Figure 12 shows pitch-averaged secondary loss and yaw angle for CFD and experiment for each geometry. Secondary loss is plotted as the CFD mid-span loss is roughly twice that of the measured value. This is caused by the CFD modelling having fully turbulent boundary layers, whereas in the real cascade the flow is transitional. Negative values of experimental loss are caused by small areas of negative loss at inlet. The negative loss at inlet arose from the fact that the inlet boundary layer had a slight 'hump' in it caused by a jetting effect from the turbulence grid and this feature of the Durham Cascade is described in more detail in Ingram [**12**].

For the *P*0 case we see that the CFD predicts the passage vortex loss core and the reduction of loss at 10–20% of span quite well, but gets some details wrong. There is a pronounced hump and dip in the CFD passage vortex loss core which does not occur in the experimental results. This appears to be a consequence of the CFD overpredicting boundary layer loss, which is then fed into the vortex associated with suction side of the horseshoe vortex and the trailing edge vorticity. The loss core associated with the passage vortex appears to be the lower 'hump' at around 25 per cent of span.

For the *P*1 case the passage vortex loss core is overpredicted in strength but the CFD does capture the increased loss associated with the enhanced corner

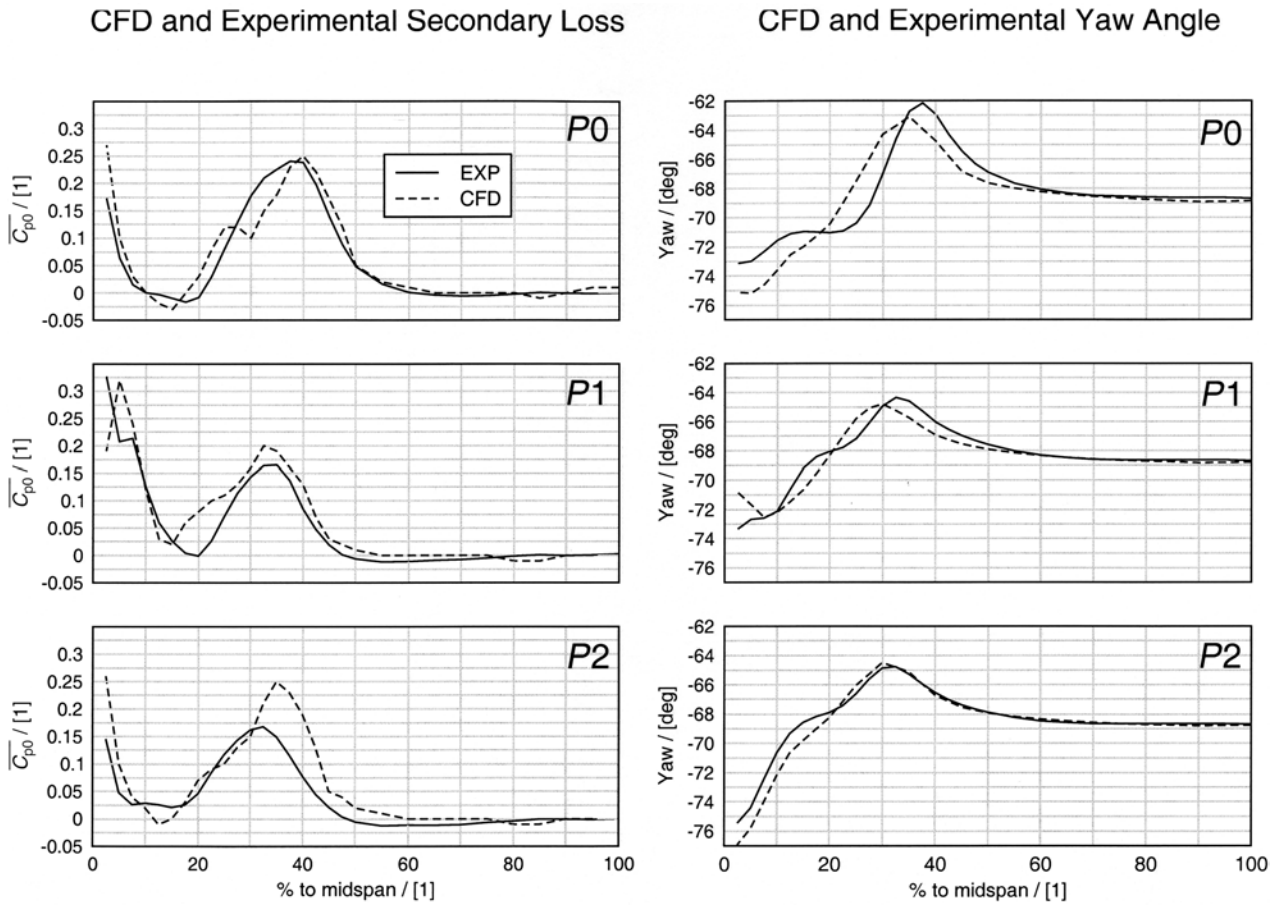

Fig. 12 Pitch-averaged experimental data compared with CFD

vortex. The dip in loss between the endwall losses and the passage vortex loss core is underpredicted, with the CFD predicting more loss than is actually present. A similar story is seen for *P*2, with the passage vortex being overpredicted and the endwall loss being captured accurately. However the dip in loss between the endwall loss and the passage vortex loss core is greater than occurs in reality.

Table 5 shows the CFD loss. This quantifies the remarks made in the previous paragraph. Secondary loss is the main parameter under consideration as this removes the effect of the blade boundary layer modelling to a great extent and the turbomachinery designer can examine secondary loss with the prior knowledge that the modelling of the mid-span flow is incorrect. However even when examining secondary loss (compared with Table 2), the CFD prediction of loss is incorrect. For *P*1 a small increase in loss is predicted and for *P*2 the loss is considerably overestimated. This is not particularly surprising, as many other experimenters have found that CFD predicts loss badly for turbomachinery applications. In a situation where loss measurement is difficult as the planar case is already quite efficient and the changes between endwalls are small, CFD would not be expected to give accurate loss results. The endwalls were designed in the expectation that the loss prediction would be poor and the profiles (*P*1 and *P*2) were designed on the basis of reducing secondary flow and not on predicted loss reduction.

Yaw angles are also shown in Fig. 12; the CFD data has been adjusted to give the same mid-span angle as the experimental data, but the size of this adjustment is very small at less than half a degree. The *P*0 case actually appears to agree the least well with the experimental data. Peak underturning and overturning are predicted in slightly the wrong places and the predicted overturning in the planar case is much greater than that which actually occurs. There is a difference of up to 2.5° between the experimental

Table 5 CFD loss predictions

	*P*0 CFD	*P*1 CFD	*P*2 CFD
Total loss, $\overline{\overline{C_{p0}}}$	0.2227	0.2212	0.2159
Mid-span loss	0.1509	0.1489	0.1491
Secondary loss	0.0716	0.0723	0.0668
Percentage planar case loss	100.0	101.0	93.3

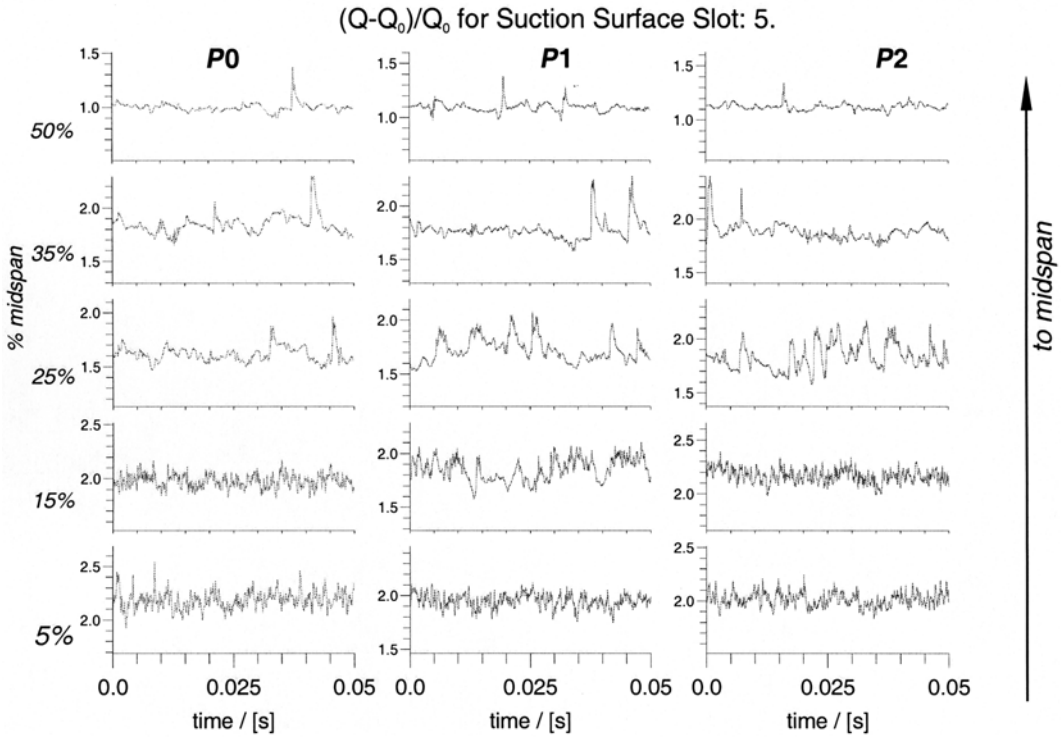

Fig. 13 Surface-mounted hot film results

results and the calculations. Predictions for the profiled endwalls appear slightly better with some discrepancies between the position of peak underturning, but the reduced overturning at the wall with *P*1 and the increased overturning at the wall for *P*2 are captured accurately.

6 HOT FILM MEASUREMENTS

Moore and Gregory-Smith [**9**] and Harrison [**14**] both showed that there are significant areas of transition on endwalls in turbine cascades. If the loss reduction caused by endwall profiling is significantly due to the changing the state of the boundary layer, its general applicability is somewhat limited. In this paper a brief selection of surface-mounted hot film results are presented.

The results of the surface-mounted hot films are available in the form of a time dependent non-dimensionalized heat transfer parameter. Figure 13 shows typical traces, here for 55 per cent axial chord on the suction surface. Near the endwall the flow is turbulent where the influence of the secondary flow is strong. Towards mid-span the flow is nearly completely laminar for the two-dimensional flow over the blade profile at this position. The differences between the three endwalls are not great, but some differences can be seen at 15 and 25 per cent span, with the profiled endwalls having a slightly more turbulent appearance. On the endwalls (not shown), the differences are not so clear between laminar and turbulent flow regions. However the readings do indicate that transition is not the major cause of the loss reduction in the blade row. The hot film measurements do show the relaminarisation described by Moore and Gregory-Smith [**9**], they used hot wires rather than hot films, so this gives confidence in the current technique. Further details may be found in Ingram [**12**].

Real machines operate at a variety of Reynolds numbers, some of which are several times higher that the Durham cascade. If the benefits of endwall profiling were derived significantly from altering the transition of the endwall or blade surface, the applicability of the technique to a wide variety of real machines would be in doubt. However the above results, along with evidence from engine representative rig tests [**6**, **7**] suggest that this is not the case.

7 CONCLUSIONS

This paper has presented details of the quantitative performance of three endwall geometries, a planar reference case and two non-axisymmetric profiled endwalls. Owing to the small differences between endwalls, ranking the profiles is quite a difficult

exercise and considerable attention must be paid to experimental technique. The following key points emerge:

- careful experimental technique is vital and, due to the small differences being measured, repetition of the experiments is advised in order to ascertain the amount of variation in the experiments;
- a quantitative ranking of three profiled endwalls has been undertaken with a realistic estimate of the error margins associated with the measurements;
- profiled endwalls have been shown to reduce secondary loss by 31 per cent with an error estimate of ± 5 per cent;
- CFD does not predict absolute values of loss for profiled endwalls nor the trends in loss production with endwall profiling. CFD does predict the yaw angle changes introduced by endwall profiling; the trends and the absolute values are captured accurately;
- increased overturning at the endwall is not necessarily accompanied by an increase in loss near the endwall;
- the transitional flow effects seen in cascades by Moore and Gregory-Smith [**9**] and Harrison [**14**] appear not to be affected by endwall profiling. This means the benefits of endwall profiling are not due to changes in the transitional state of the boundary layers.

ACKNOWLEDGEMENTS

This work has been carried out with the support of Rolls-Royce plc, QinetiQ, MoD, and DTI CARAD. The authors would like to thank them for funding it and their permission to publish this paper.

REFERENCES

1 **Sieverding, C. H.** Recent progress in the understanding of basic aspects of secondary flows in turbine blade passages. *ASME J. Engng Gas Turbines Power*, 1985, **107**, 248–252.

2 **Harvey, N. W., Rose, M. G., Shahpar, S., Taylor, M. D., Hartland, J.,** and **Gregory-Smith, D. G.** Non-axisymmetric turbine end wall design: Part I. Three-dimensional design system. *ASME J. Turbomachin.*, 2000, **122**, 278–285.

3 **Hartland, J., Gregory-Smith, D. G., Harvey, N. W.,** and **Rose, M. G.** Non-axisymmetric end wall design: Part II. Experimental validation, ASME paper 99-GT-338. *ASME J. Turbomachin.*, 2000, **122**, 286–293.

4 **Yan, J., Gregory-Smith, D. G.,** and **Walker, P.J.** Secondary flow reduction in a nozzle guide vane cascade by non-axisymmetric end-wall profiling. ASME paper 99-GT-339, 1999.

5 **Brennan, G., Harvey, N. W., Rose, M. G., Formison, N.,** and **Taylor, M. D.** Improving the efficiency of the Trent 500 HP turbine using non-axisymmetric end walls: part 1. Turbine design. ASME paper 2001-GT-0444, 2001.

6 **Rose, M. G., Harvey, N. W., Seaman, P., Newman, D. A.,** and **McManus, D.** Improving the efficiency of the Trent 500 HP turbine using non-axisymmetric end walls: Part 2. Experimental validation. ASME paper 2001-GT-0505, 2001.

7 **Harvey, N. W., Brennan, G., Newman, D. A.,** and **Rose, M. G.** Improving turbine efficiency using non-axisymmetric endwalls: validation in the multi-row environment and with low aspect ratio blading. ASME paper GT-2002-30337, 2002.

8 **Ingram, G. L., Gregory-Smith, D. G., Rose, M. G., Harvey, N. W.,** and **Brennan, G.** The effect of endwall profiling on secondary flow and loss development in a turbine cascade. ASME paper GT-2002-30339, 2002.

9 **Moore, H.** and **Gregory-Smith, D. G.** Transition effects on secondary flows in a turbine cascade. ASME paper 96-GT-100, 1996.

10 **Gregory-Smith, D. G., Ingram, G., Jayaraman, P., Harvey, N. W.,** and **Rose, M. G.** Non-axisymmetric turbine end wall profiling. In Proceedings of the 4th European Conference on *Turbomachinery*, Florence, March 20–23, 2001, pp. 653–664.

11 **Treaster, A. I.** and **Yocum, A. M.** The calibration and application of five hole probes. *ISA Trans.*, 1979, **18**(2), 23.

12 **Ingram, G. L.** Endwall profiling for the reduction of secondary flow in turbines, PhD Thesis, University of Durham, 2003.

13 **Moore, J. G.** Calculation of 3D flow without numerical mixing. In *3D Computation Techniques Applied to Internal Flows in Propulsion Systems*, 1985, AGARD-LS-140, pp. 8.1–8.15.

14 **Harrison, S.** Secondary loss generation in a linear cascade of high-turning turbine blades. *J. Turbomachin.*, 1990, **112**, 618–624.

APPENDIX

Notation

C_{ax}	axial chord
C_{p0}	loss coefficient, (local total pressure − upstream total pressure)/inlet dynamic head
$\overline{C_{p0}}$	pitch averaged loss coefficient
$\overline{\overline{C_{p0}}}$	area averaged loss coefficient
C_{ske}	secondary kinetic energy coefficient, referenced to inlet velocity
$P0$	planar endwall
$P1$	first-generation profiled endwall
$P2$	second-generation profiled endwall
r	radial coordinate
t	tangential coordinate